Pergamon

Int. J. Heat Mass Transfer. Vol. 39, No. 7, pp. 1479–1488, 1996

0017–9310/96 $15.00 + 0.00

0017–9310(95)00227–8

Combined buoyancy effects of thermal and mass diffusion on laminar forced convection in horizontal rectangular ducts

WEI-MON YAN

Department of Mechanical Engineering, Hua Fan College of Humanities and Technology, Shih Ting, Taipei, Taiwan 22305, Republic of China

(*Received* 1 *September* 1992 *and in final form* 13 *March* 1995)

Abstract—This paper presents a numerical study of mixed convection heat and mass transfer in horizontal rectangular ducts. The vorticity-velocity method with the Du Fort Frankel scheme is employed to solve the governing equations for the flow, heat and mass transfer. Variations in local friction factor ratio, Nusselt number and Sherwood number with different parameters are shown for species diffusion of interest in air ($Pr = 0.7$) over a Schmidt number range of $Sc = 0.2$–2.0. In this work, the Rayleigh numbers are varied from 0 to 10^5 for aspect ratios 0.5, 1 and 2 with buoyancy ratios ranging from -0.8 to 2.0. The results show that the distributions of local Nusselt (Sherwood) number are characterized by a decay near the inlet in which the forced-convection entrance effect dominates; but the decay is attenuated by the onset of buoyancy-driven secondary flow. After a local minimum being researched, maximum and minimum local Nusselt (Sherwood) numbers may exist for some cases. Finally, the *Nu* (*Sh*) falls asymptotically to the value of Graetz problem when the bulk temperature (concentration) approaches the wall temperature (concentration). Additionally, the $f\,Re$, *Nu* and *Sh* are found to increase and decrease as the buoyancy force from species diffusion assists and opposes, respectively, the thermal buoyancy force.

1. INTRODUCTION

Transport processes, in which the simultaneous buoyancy forces of heat and mass transfer have considerable influences on the momentum, heat and mass transfer in a flowing gas mixture, are often encountered in many engineering systems and natural environments. Noticeable examples include the chemical distillatory processes, design of heat exchangers, channel type solar energy collectors and thermo-protection systems. Hence, the effects of combined buoyancy forces due to the variations of temperature and concentration on the laminar forced convection in horizontal rectangular ducts are relatively important.

A vast amount of work, both theoretical and experimental, exists in the literature to examine the thermal buoyancy effects on the forced convection heat transfer in horizontal ducts. Only those relevant to the present work are briefly reviewed here. The fully-developed mixed convection heat transfer in horizontal rectangular ducts has been investigated by Cheng and Hwang [1] and Chou and Hwang [2]. The heat transfer enhancement in laminar fully developed channel flow by means of heating from below was experimentally examined by Ostrach and Kamotani [3]. But these results are limited to a long channel, only.

Employing the assumption of large Prandtl number, Cheng *et al.* [4], Ou *et al.* [5] and Cheng and Ou [6] have studied the mixed convection heat transfer in the thermal entrance region of horizontal rectangular channels. The same problems were also examined for a horizontal tube by Hieber and Sreenivasan [7], Hong *et al.* [8], Ou and Cheng [9] and Hishida *et al.* [10]. Their results showed that the secondary flow induced by the thermal buoyancy force can enhance significantly the heat transfer. In addition, the buoyancy would decrease the thermal entrance length.

By using large Prandtl number assumption, the inertia terms in the momentum equations are neglected. That is, the secondary flow is not significant in the momentum equations but is important in the energy equation. However, the results are obviously not applicable to both moderate and small Prandtl number fluids. Without the assumption of large Prandtl number, the detailed numerical studies on mixed convection heat transfer in horizontal ducts or pipes have been investigated by Abou-Ellai and Morcos [11], Incropera and Schutt [12], Mahaney *et al.* [13], Chou and Hwang [14, 15], Lin and Chou [16] and Lin *et al.* [17]. Experimental studies for mixed convection heat transfer in the horizontal channels have been investigated by Hwang and Liu [18], Kamotani *et al.* [19] and Maughan and Incropera [20].

The effects of combined buoyancy forces of heat and mass diffusion on laminar forced convection heat transfer in a vertical parallel-plate channel or pipe were well studied. Santarelli and Foraboschi [21] examined the buoyancy effects on laminar forced convection flow undergoing a chemical reaction. The

NOMENCLATURE

A cross-sectional area of a horizontal rectangular duct [m^2]
a, b width and height of a rectangular duct, respectively [m]
c, C dimensional and dimensionless species concentration, respectively
D mass diffusivity
D_e equivalent hydraulic diameter, $4A/S$
f friction factor, $2\bar{\tau}_w/(\rho_o \bar{w}_f^2)$
g gravitational acceleration [m s^{-2}]
Gr Grashof number, $g\beta(T_w - T_o)D_e^3/\nu^2$
I, J number of finite difference divisions in X and Y directions, respectively
$\bar{h}$ average heat transfer coefficient [W m^{-2}K^{-1}]
$\bar{h}_M$ average mass transfer coefficient
m mth iteration
N buoyancy ratio, $\beta^*(c_w - c_o)/[\beta(T_w - T_o)]$
Nu local Nusselt number, $\bar{h}D_e/k$
p_m dynamic pressure [kPa]
$\bar{p}$ cross-sectional mean pressure [kPa]
$\bar{P}$ dimensionless cross-sectional mean pressure
P' perturbation term about the mean pressure $\bar{P}$
Pr Prandtl number, ν/α
Ra Rayleigh number, $PrGr$
Re Reynolds number, $\bar{w}_f D_e/\nu$
S circumference of cross section [m]
Sc Schmidt number, ν/D
Sh Sherwood number, $\bar{h}_m D_e/D$
T temperature [K]
T_o inlet temperature [K]
T_w wall temperature [K]
U, V, W dimensionless velocity components in the X, Y and Z directions, respectively
w_f fully-developed axial velocity before the entrance [m s^{-1}]
W_f dimensionless fully-developed axial velocity before thermal entrance
$\bar{W}_f$ mean quantity for W_f
x, y, z rectangular coordinate [m]
X, Y, Z dimensionless rectangular coordinate, $X = x/D_e$, $Y = y/D_e$, $Z = z/(ReD_e)$
Z^* dimensionless z-direction coordinate, $z/(PrReD_e) = Z/Pr$.

Greek symbols
α thermal diffusivity [m^2 s^{-1}]
β coefficient of thermal expansion [1/K]
β^* coefficient of concentration expansion
γ aspect ratio of a rectangular duct, a/b
θ dimensionless temperature, $(T - T_o)/(T_w - T_o)$
ν kinematic viscosity [m^2 s^{-1}]
ξ dimensionless vorticity in axial direction
ρ density [kg m^{-3}].

Subscripts
b bulk fluid quantity
f fully-developed quantity before thermal entrance
o condition for purely forced convection
w value at wall.

effects of wetted wall on laminar mixed convection heat and mass transfer in a vertical pipe were performed by Lin *et al.* [22]. In their analyses, they found that the buoyancy forces have considerable effects on laminar forced convection. Recently, mixed convection heat and mass transfer in a horizontal square duct has been studied by Lin *et al.* [23]. In ref. [23], a uniform temperature and uniform concentration is assumed along the bottom wall of a square rectangular duct. While the other walls, a zero heat and mass flux (i.e. insulated) is assumed. In addition, the flowing gas mixture is limited to the air–water vapor mixture.

Regardless of its importance in engineering applications, the mixed convection heat and mass transfer in horizontal rectangular ducts has not been well evaluated. This motivates the present investigation. The purpose of this study is to examine the effects of combined buoyancy forces of thermal and mass diffusion in horizontal rectangular channels.

2. ANALYSIS

2.1. *Problem statement*

The geometry of the system to be examined, as schematically shown in Fig. 1, is a horizontal rectangular duct. The walls are kept at a uniform temperature T_w and uniform concentration c_w. The u, v

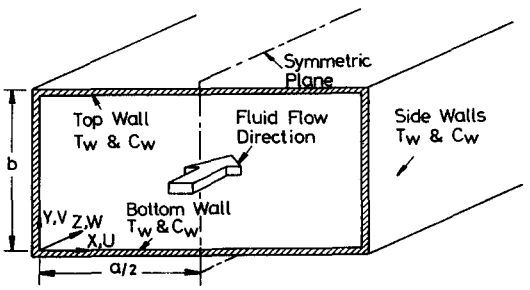

Fig. 1. Physical configuration and coordinate system.

and w are the velocity components in the x, y and z directions, respectively. A fully-developed axial velocity profiles w_f is imposed at the entrance $z = 0$. The fluid at the entrance $z = 0$ has a constant temperature T_o and concentration c_o. The flow is assumed to be steady and have constant thermophysical properties except the buoyancy term in the y momentum equation. The buoyancy force resulting from the concentration difference may assist or oppose the buoyancy force from the temperature variations in the fluid. To facilitate the analysis, an order of magnitude analysis is employed which deduces the governing equations by neglecting the axial diffusion of momentum, heat and mass [12–14]. Because of the symmetry inherent in the problem, the calculations can be restricted to a solution domain that comprises one-half of the horizontal rectangular duct as shown in Fig. 1.

2.2. *Governing equations*

The governing equations are those of conservation of mass, momentum, energy and concentration. The pressure gradient and body force terms in the transverse momentum equations are:

$$-\partial p/\partial y - \rho g. \tag{1}$$

By using the equation of state for an ideal gas mixture and assuming a low level of concentration in the flow, the density variation in the flow can be approximated by

$$\rho = \rho_o[1-\beta(T-T_o)-\beta^*(c-c_o)] \tag{2}$$

where ρ_o is the density evaluated at the reference temperature T_o and concentration c_o. With a dynamic pressure p_m defined as

$$p_m = p - \rho_o g y \tag{3}$$

equation (1) may be rewritten as

$$-\partial p_m/\partial y + \rho_o g\beta(T-T_o) + \rho_o g\beta^*(c-c_o). \tag{4}$$

The flow is assumed to be parabolic [12–14] and in the axial momentum equation a space-averaged pressure $\bar{p}$ is imposed to prevail at each cross section, thus permitting a decoupling from the pressure p_m in the cross-sectional momentum equations. This 'pressure uncoupling' follows the parabolic-flow practice and, together with the neglect of axial diffusion of momentum, heat and concentration by an order of analysis, permits a marching-integration calculation procedure. To conveniently present the governing equations, the dynamic pressure p_m can be represented as the sum of a cross-section mean pressure $\bar{p}(z)$, which derives the main flow, and a perturbation about the mean, $p'(x, y)$, which derives the cross stream flow,

$$p_m = \bar{p}(z) + p'(x, y). \tag{5}$$

As a final step, dimensionless variables are introduced as follows:

$$\begin{aligned}
&X = x/D_e && Y = y/D_e \\
&Z = z/(ReD_e) && Z^* = Z/Pr \\
&U = u\cdot D_e/\nu && V = vD_e/\nu \\
&W = w/\bar{w}_f && \bar{P} = \bar{p}/(\rho_o \bar{w}_f^2) \\
&P' = p'/(\rho_o \nu^2/D_e^2) && \theta = (T-T_o)/(T_w-T_o) \\
&C = (c-c_o)/(c_w-c_o) && Gr = g\beta(T_w-T_o)D_e^3/\nu^2 \\
&Ra = PrGr && N = \beta^*(c_w-c_o)/[\beta(T_w-T_o)] \\
&Pr = \nu/\alpha && Sc = \nu/D \\
&\gamma = a/b && D_e = 4A/S.
\end{aligned} \tag{6}$$

With these definitions and the assumptions made earlier, the non-dimensional governing equations are: continuity equation:

$$\partial U/\partial X + \partial V/\partial Y + \partial W/\partial Z = 0 \tag{7}$$

x-direction momentum equation:

$$U\partial U/\partial X + V\partial U/\partial Y + W\partial U/\partial Z = -\partial P'/\partial X + \partial^2 U/\partial X^2 + \partial^2 U/\partial Y^2 \tag{8}$$

y-direction momentum equation:

$$U\partial V/\partial X + V\partial V/\partial Y + W\partial V/\partial Z = -\partial P'/\partial Y + \partial^2 V/\partial X^2 + \partial^2 V/\partial Y^2 + (Ra/Pr)\cdot(\theta + NC) \tag{9}$$

z-direction momentum equation:

$$U\partial W/\partial X + V\partial W/\partial Y + W\partial W/\partial Z = -\mathrm{d}\bar{P}/\mathrm{d}Z + \partial^2 W/\partial X^2 + \partial^2 W/\partial Y^2 \tag{10}$$

energy equation:

$$U\partial\theta/\partial X + V\partial\theta/\partial Y + W\partial\theta/\partial Z = (\partial^2\theta/\partial X^2 + \partial^2\theta/\partial Y^2)/Pr \tag{11}$$

concentration equation:

$$U\partial C/\partial X + V\partial C/\partial Y + W\partial C/\partial Z = (\partial^2 C/\partial X^2 + \partial^2 C/\partial Y^2)/Sc. \tag{12}$$

The non-dimensional axial vorticity can be expressed as

$$\xi = \partial U/\partial Y - \partial V/\partial X. \tag{13}$$

The axial vorticity transport equation can be derived from equations (8) and (9) as

$$\begin{aligned}
&U\partial\xi/\partial X + V\partial\xi/\partial Y + W\partial\xi/\partial Z \\
&\quad + \xi(\partial U/\partial X + \partial V/\partial Y) + (\partial W/\partial Y\cdot\partial U/\partial Z \\
&\quad - \partial W/\partial X\cdot\partial V/\partial Z) \\
&= \partial^2\xi/\partial X^2 + \partial^2\xi/\partial Y^2 - (Ra/Pr) \\
&\quad \cdot(\partial\theta/\partial X + N\partial C/\partial X).
\end{aligned} \tag{14}$$

The equations of the transverse velocity components (U, V) can be derived from the continuity,

equation (7), and the definition of axial vorticity, equation (13), as

$$\partial^2 U/\partial X^2+\partial^2 U/\partial Y^2 = \partial\xi/\partial Y-\partial^2 W/\partial X\,\partial Z \quad (15)$$

$$\partial^2 V/\partial X^2+\partial^2 V/\partial Y^2 = -\partial\xi/\partial X-\partial^2 W/\partial Y\,\partial Z. \quad (16)$$

2.3. *Boundary conditions*

As mentioned earlier, because of the symmetry about the symmetric plane as shown in Fig. 1, it is sufficient to solve the equations over only the left-hand side of the horizontal rectangular duct. Conditions of interest in this work are
duct walls:

$$U = V = W = 0, \quad \theta = C = 1 \quad (17a)$$

midplane $[X = (1+\gamma)/4]$:

$$\partial W/\partial X = U = \partial V/\partial X = \partial\theta/\partial X = \partial C/\partial X = 0 \quad (17b)$$

entrance $(Z = 0)$:

$$W = W_f, \quad U = V = \xi = \theta = C = 0. \quad (17c)$$

The interfacial velocity at the duct walls as a result of mass diffusion process will be neglected in the analysis. This is because consideration will be given to situations in which the concentration level is low. The validity and the condition for the neglect of interfacial velocity has been discussed in refs. [24, 25]. In the study of duct flow, the overall mass flow rate at every axial location must be balanced in the duct flow,

$$\int_0^{(1+\gamma)/(2\gamma)}\int_0^{(1+\gamma)/4} W\,dX\,dY = (1+\gamma)^2/(8\gamma). \quad (18)$$

This equation is used to deduce the pressure gradient in the axial momentum equation, equation (10).

2.4. *Governing parameters*

The governing equations contain five dimensionless parameters: *Ra*, *N*, γ, *Pr* and *Sc*. Buoyancy ratio *N* represents the relative effect of chemical species diffusion on the thermal diffusion. When $N = 0$, there is no mass diffusion effect and the buoyancy force arises solely from the temperature difference. The buoyancy forces from mass and thermal diffusion are combined to assist the flow when as $N > 0$, whereas they oppose each other as $N < 0$. In this work, the results are presented for species diffusion in air ($Pr = 0.7$) with Schmidt numbers ranging from 0.2 to 2.0. This covers diffusion into air of hydrogen ($Sc = 0.22$), water vapor (0.6), ethanol vapor (1.3) and benzene vapor (2.01) [24, 25]. The Rayleigh numbers *Ra* were varied between 0 and 10^5 for aspect ratios γ 0.5, 1.0 and 2.0 with buoyancy ratios *N* from -0.8 to 2.

3. SOLUTION METHOD

The governing equations are solved by the vorticity-velocity method for three-dimensional (3D) parabolic flow [26]. The equations for the unknowns *U*, *V*, *W* ξ, θ, *C* and $d\bar{P}/dZ$, equations (10)–(12) and (14)–(16) satisfying boundary conditions (17), are coupled. A numerical finite-difference scheme based on the vorticity-velocity method is used to obtain the solution of equations (10)–(12) and (14)–(16). The solution procedure is as follows:

(1) The axial velocity at the entrance ($Z = 0$), constrained to $\bar{W}_f = 1$, is solved independently using the S.O.R. method.

(2) The initial values of *U*, *V*, θ and *C* are assigned to be zero at the entrance.

(3) For any axial location, with the known values of *U*, *V* and assigned $(d\bar{P}/dZ)$, the axial velocity *W* at the current position is obtained from equation (10), with constraint (18) to meet the requirement of constant flow rate.

(4) With the known values of *U*, *V* and *W*, the equations (11), (12) and (14) for θ, *C* and ξ subjected to the boundary conditions can be solved by the Du Fort–Frankel method [27].

(5) The values of $\partial^2 W/\partial X\,\partial Z$, $\partial^2 W/\partial Y\,\partial Z$, $\partial\xi/\partial Y$ and $\partial\xi/\partial X$ in equations (15) and (16) are calculated by using backward differences axially and central difference in the transverse directions. The elliptic-type equations (15) and (16) are then solved for *U* and *V* by iteration. During the iteration process, the values of vorticity on the boundary are evaluated simultaneously with *U* and *V* in the interior region. The boundary vorticity can be evaluated with an expression given in ref. [14].

(6) Steps (3)–(5) are repeated at a cross-section until the following criterion is satisfied for the velocity components *U* and *V*,

$$\varepsilon = \mathrm{Max}\,|\phi_{i,j}^{m+1}-\phi_{i,j}^{m}|/\mathrm{Max}\,|\phi_{i,j}^{m+1}| < 10^{-5}, \quad \phi = U \text{ or } V \quad (19)$$

where *m* is the *m*th iteration of steps (3)–(5).

(7) Steps (3)–(6) are repeated at each axial location from the entrance to the downstream of interest.

In this work, the uniform cross-sectional meshes were chosen, while the *z* direction grid spacing was nonuniform with grid lines being more closely packed near the entrance ($Z = 0$). The axial step size ΔZ^* was varied from 2×10^{-5} near the duct entrance to about 2×10^{-4} near the fully-developed region. Grid independence tests both in the cross-sectional direction and axial direction have been performed for a typical case of $Pr = 0.7$, $Ra = 5\times10^4$, $N = 1$, $Sc = 0.6$ and $\gamma = 1$. Three arrangements of grid points in the *x*, *y* and *z* directions are tested and corresponding results are presented in Table 1. It is found that the deviations in *Nu* calculated with $I\times J = 16\times32$ and 20×40 ($\Delta Z^* = 2\times10^{-5}$–$2\times10^{-4}$) are always less than 2%. Furthermore, the deviations in *Nu* cal-

Table 1. Comparisons of local Nusselt number for different mesh size ($I \times J$) and axial step size (ΔZ^*) for $Ra = 5 \times 10^4$, $N = 1$, $Sc = 0.6$ and $\gamma = 1$

	Z^*						
$I \times J$ (ΔZ^*)	Nu						
	0.001	0.004	0.010	0.030	0.070	0.150	0.40
16×32 (2×10^{-5}–2×10^{-4})	9.383	6.503	6.857	7.161	5.912	4.281	3.305
20×40 (2×10^{-5}–2×10^{-4})	9.368	6.445	6.748	7.123	5.912	4.316	3.048
16×32 (5×10^{-6}–2×10^{-4})	9.374	6.471	6.823	7.151	5.912	4.280	3.034

culated using $I \times J$ (ΔZ^*) = 16×32 (5×10^{-6}–2×10^{-4}) and 16×32 (2×10^{-5}–2×10^{-4}) are all less than 2%. Accordingly, the computations involving a $I \times J$ (ΔZ^*) = 16×32 (2×10^{-5}–2×10^{-4}) grid are considered to be sufficiently accurate to describe the heat and mass transfer in a horizontal rectangular duct. All the results presented in the next section are computed using the latter grid.

As a partial verification of the computational procedure, results were initially obtained for mixed convection heat transfer in a horizontal rectangular duct with $Pr = 0.7$, $Ra = 6 \times 10^4$ and $\gamma = 1.0$. The results for heat transfer were compared with those of Chou and Hwang [14]. The Nusselt numbers were found to agree within 1%. Additionally, the results of limiting case of forced convection were calculated and compared with those of Shah and London [28]. Excellent agreement was obtained. Through these validation procedures, the above solution method is suitable for the present problem.

4. RESULTS AND DISCUSSION

4.1. *Axial distributions of friction factor, Nusselt and Sherwood numbers*

The results of the local pressure gradient in the entrance region of the horizontal rectangular duct may be presented through the value of dimensionless friction factor

$$f Re/(f Re)_o = (d\bar{P}/dZ)/(d\bar{P}/DZ)_o \quad (20)$$

where the subscript o denotes the quantity for forced convection without buoyancy effects. The value is available in ref. [28].

The Nusselt and Sherwood numbers are of importance because they are directly related to the heat and mass transfer coefficients. The cross-sectional averaged Nusselt and Sherwood numbers can be evaluated by considering the overall energy and concentration balance for axial length, dZ,

$$Nu = [Pr/(1-\theta_b)] \cdot (\partial\theta_b/\partial Z) \quad (21)$$

$$Sh = [Sc/(1-C_b)] \cdot (\partial C_b/\partial Z) \quad (22)$$

4.1.1. *Effects of Rayleigh Number* Ra. Figure 2 presents the axial variations of $(f Re)/(f Re)_o$ for different Rayleigh number Ra at $\gamma = 1$, $N = 1$, $Sc = 0.6$ and $Pr = 0.7$. It is clear that the buoyancy effect is negligible up to a certain axial distance Z^*. This axial distance depends primarily on the magnitude of the Rayleigh number: the greater is Ra, the shorter is the distance. Since the development of successive strengthening and weakening of the secondary flow is repeated, the value of $f Re/(f Re)_o$ appears an oscillatory phenomenon when Ra becomes large. After reaching their maximum values, the curves of $f Re/(f Re)_o$ then gradually approach 1 as the bulk fluid temperature and concentration approach the wall temperature and concentration. The occurrence of maximum local friction factor is closely related to the appearance of local maximum secondary flow intensity [12, 16]. Also found in Fig. 2 is that the increase in the value of $f Re$ over the forced convection value of $(f Re)_o$ can be as much as 75% for $Ra = 10^5$.

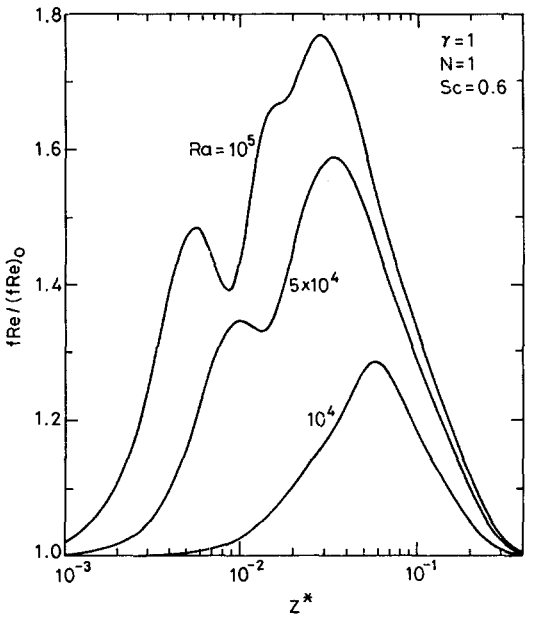

Fig. 2. The axial variations of the local friction factor ratio for $N = 1$, $Sc = 0.6$ and $\gamma = 1$ with Ra as parameter.

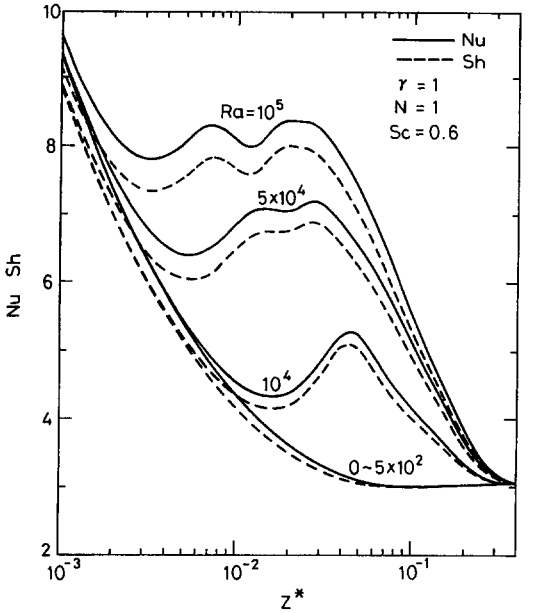

Fig. 3. The axial variations of the local Nusselt and Sherwood numbers for $N = 1$, $Sc = 0.6$ and $\gamma = 1$ with Ra as parameter.

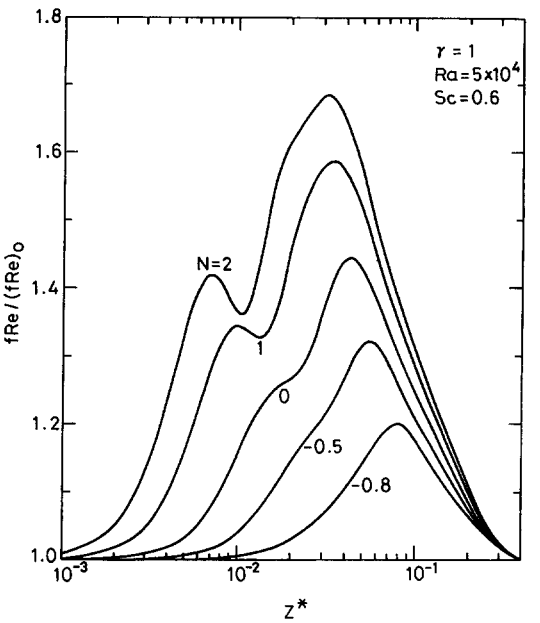

Fig. 4. The axial variations of the local friction factor ratio for $Ra = 5 \times 10^4$, $Sc = 0.6$ and $\gamma = 1$ with N as parameter.

Longitudinal distributions of the peripherally average Nusselt and Sherwood numbers are shown in Fig. 3. Referring to the near-entry region, the results are seen to provide a monotonic decay in Nu and Sh. This is attributed to the entrance effect. The initial increase in Nu (Sh) above the corresponding curve of forced convection is owing to the formation of buoyancy-driven secondary flow. However, the Nu (Sh) continues to decline with increasing Z^*. The first minimum in the Nu (Sh) distribution is reached when the reduction in Nu (Sh) due to forced convection entrance effect is balanced out by an increase owing to the buoyancy-driven secondary flow. After reaching the first minimum in Nu (Sh), two oscillations occur as the flow goes downstream for $Ra = 5 \times 10^4$ and 1×10^5. The results then gradually approach an asymptotic situation. The first minimum in the Nu (Sh) and the subsequently oscillatory phenomena are also found in the results of mixed convection heat transfer in a horizontal duct [13, 17]. The oscillations for Nu and Sh are attributed to the successive strengthening and weakening of the secondary flow being repeated. In addition, the variation of the Sh resembles that of Nu because Pr ($= 0.7$) is close to Sc (0.6). It is worth noting that in this study the free convection effect is practically insignificant for $Ra \leqslant 5 \times 10^2$. This clearly demonstrates that the forced convection result is a limiting case and applicable only when $Ra \leqslant 5 \times 10^2$.

4.1.2. *Effects of buoyancy ratio* N. The effects of buoyancy ratio N on the variations of local $f Re/(f Re)_o$, Nu and Sh are presented in Figs. 4 and 5. The buoyancy ratio N represents the ratio of the concentration to thermal buoyancy. It is clear that as compared to the case of $N = 0$ (i.e. the case in which there is no mass diffusion effect and the buoyancy force arises only from the thermal variations), the local friction factor, Nusselt and Sherwood numbers increase when the buoyancy force from species diffusion acts in the same direction of the thermal buoyancy force (i.e. as $N > 0$) and decrease when the solutal buoyancy force acts in the opposite direction of the thermal buoyancy force (i.e. as $N < 0$). Indeed, the combined effects of thermal and solutal diffusion are represented by the term $\theta + NC$ in equation (9).

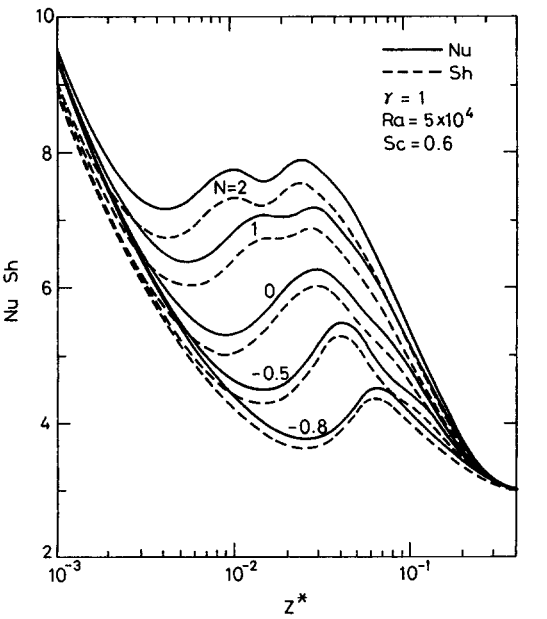

Fig. 5. The axial variations of the local Nusselt and Sherwood numbers for $Ra = 5 \times 10^4$, $Sc = 0.6$ and $\gamma = 1$ with N as parameter.

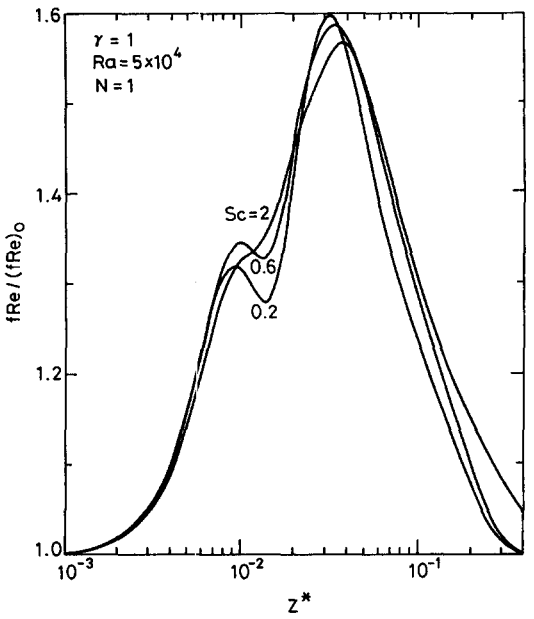

Fig. 6. The axial variations of the local friction factor ratio for $Ra = 5 \times 10^4$, $N = 1$ and $\gamma = 1$ with Sc as parameter.

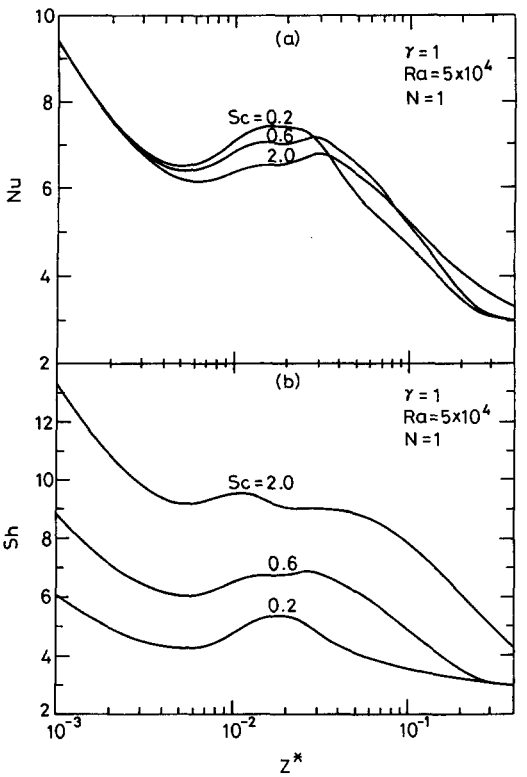

Fig. 7. The axial variations of the local Nusselt and Sherwood numbers for $Ra = 5 \times 10^4$, $N = 1$ and $\gamma = 1$ with Sc as parameter.

When the combination of Pr, Sc, Ra, N and γ is such that $\theta + NC > \theta$, the net buoyancy force contributes to an increase in the friction factor, Nusselt and Sherwood numbers beyond their respective values for $N = 0$. On the other hand, if $\theta + NC < \theta$, the net buoyancy force will contribute to a decrease in these three quantities below those for $N = 0$. Inspection of Figs. 4 and 5 further indicates that the location at which enhancement begins advances upstream with increasing N. This effect is due to the increase in the combined buoyancy effects of thermal and solutal diffusion.

4.1.3. *Effects of Schmidt number* Sc. Figures 6 and 7 give the effects of Schmidt number on the local friction factor, Nusselt and Sherwood numbers. Overall inspection on Figs. 6 and 7 discloses that the axial location of the occurrence of the onset of buoyancy effect is almost independent of the value of Schmidt number Sc. Moreover, under the range of $Sc = 0.2$ to 2, the development of the flow, heat and mass transfer is slower for the system with a larger Schmidt number Sc. Closer inspection on Figs. 7(a) and (b) reveals that the axial location of the first minimum of the local Nu (Sh) advances upstream for a smaller Sc. In addition, larger values of Schmidt number Sc are seen to provide larger Sherwood number Sh. This is due to the fact that a larger Schmidt number corresponds to a smaller binary diffusion coefficient for a given mixture and to a thinner concentration boundary layer relative to the momentum boundary layer. This results in a larger mass transfer rate at the duct walls or a larger Sherwood number.

4.1.4. *Effects of aspect ratio* γ. The effect of the aspect ratio of a rectangular duct on the variations of the $f\,Re/(f\,Re)_o$, Nu and Sh is of practical interest. The local variations of the $f\,Re/(f\,Re)_o$ for aspect ratios $\gamma = 0.5$ and 2 are shown in Fig. 8. Comparing Figs. 2 and 8, it is found that the behavior of the $f\,Re/(f\,Re)_o$ for aspect ratio $\gamma = 0.5$ and 2.0 is qualitatively similar to that of $\gamma = 1$. However, the maximum values of the $f\,Re/(f\,Re)_o$ of square channel (i.e. $\gamma = 1$) are higher than those with other aspect ratios. Figures 9(a) and (b) are the local distributions of Nusselt number for $\gamma = 0.5$ and $\gamma = 2.0$, respectively. In each of these two figures, the lowest curve can be regarded as a limiting case for pure forced convection. With further comparison with Fig. 3, one can observe that the heat transfer performance in the channel with smaller aspect ratio $\gamma = 0.5$ is better than those for other aspect ratio ($\gamma = 1$ or $\gamma = 2.0$). This is due to the heated side-wall effect, which is more significant when aspect ratio is small. The side walls induce a strong secondary flow in the region near the side walls [16].

As mentioned earlier, the local Nusselt number variations reveal that the onset of secondary flow effect due to buoyancy forces occurs at a certain entrance distance depending on the value of Rayleigh number or buoyancy ratio. Up to the onset point, the Graetz theory applies. In this respect, the onset of secondary flow effect is of practical interest in design. In the work, a 2% deviation of local Nusselt number from the value for pure forced convection was used as the criterion for onset of the thermal instability. This criterion was also used by Ou *et al.* [5] and Lin *et al.* [17] to study the onset of the thermal instability. Figure 10

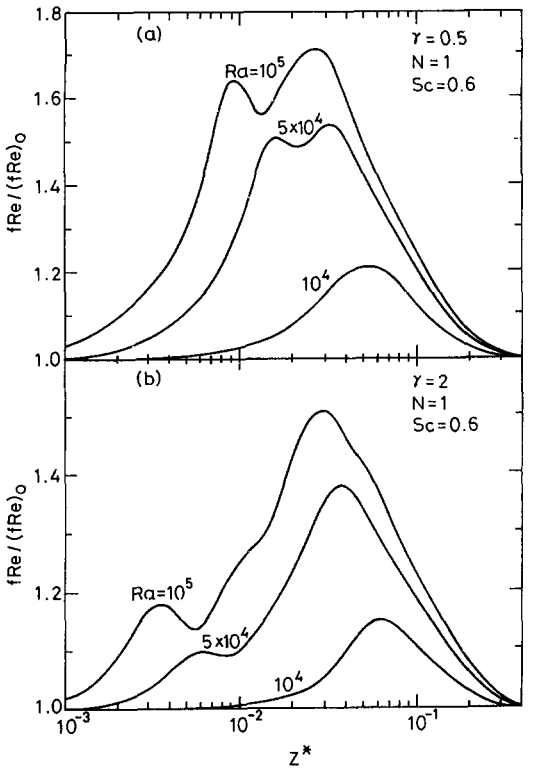

Fig. 8. The axial variations of the local friction factor ratio with Ra as parameter for (a) $\gamma = 0.5$, (b) $\gamma = 2.0$.

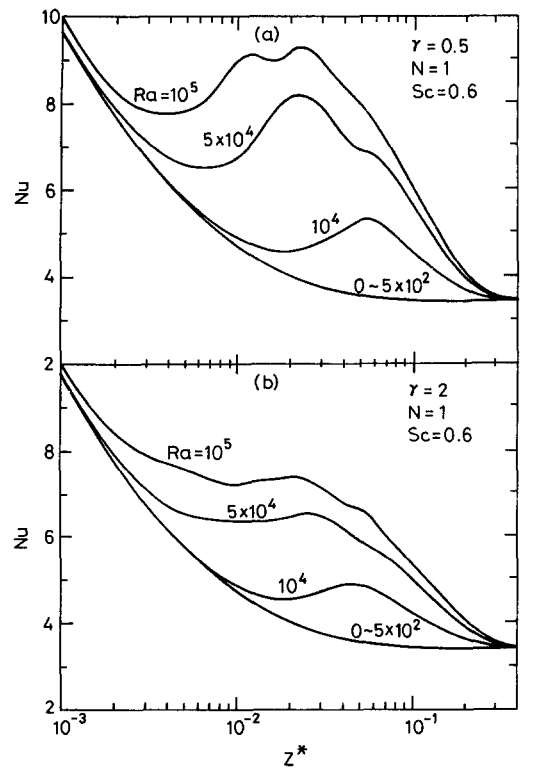

Fig. 9. The axial variations of the local Nusselt number with Ra as parameter for (a) $\gamma = 0.5$, (b) $\gamma = 2.0$.

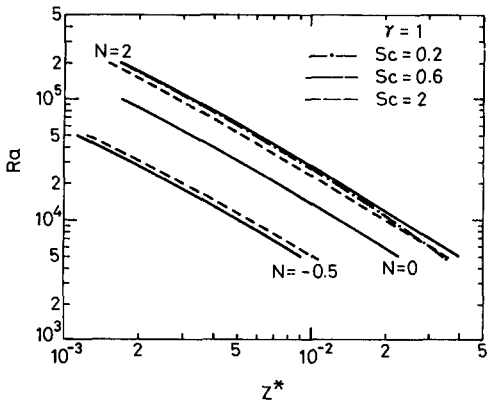

Fig. 10. The effects of buoyancy ratio and Schmidt number on the axial locations for 2% increase of local Nusselt number.

gives the effects of the buoyancy ratio N and Schmidt number Sc on the axial locations for 2% increase of local Nusselt number. In Fig. 10, the onset points advance when the solutal buoyancy force assists the thermal buoyancy force ($N = 2$). Moreover, the effect of Schmidt number Sc on the axial locations for 2% increase of local Nusselt number is insignificant.

4.2. *Developments of axial velocity, temperature and concentration*

Although the presentation of the local friction factor, Nusselt number and Sherwood number in mixed convection heat and mass transfer is a major goal in this work, developments of axial velocity, temperature and concentration profiles are of engineering interest and useful in clarifying the heat and mass transfer mechanism. Figure 11 shows the developments of axial velocity along the vertical center plane $x = a/2$. It is well known that the axial velocity profiles for purely forced convection without buoyancy effects are symmetric with respect to the $Y = 0.5$ line. Overall inspection of Fig. 11 indicates that near the entrance, the velocity profile (curve A) is symmetric and parabolic. But as the flow goes downstream, this symmetry is lost and the locations of the maximum axial velocity move toward the bottom wall. This is attributed to the buoyancy-driven secondary flow. Farther downstream, the developing W profile approaches the fully-developed profile due to the decrease of buoyancy-driven secondary flow. It was found in the separate numerical runs that as $Z^* = 1$, the developing W profile coincides with curve A. To investigate the effects of buoyancy ratio N, the developing W profile for the case of $N = -0.5$ is presented in Fig. 11(b). Comparing the corresponding curves in Figs. 11(a) and (b), it was found that the buoyancy ratio N has a pronounced effect on the distributions of axial velocity. The decrease of N from $N = 1$ to -0.5 makes the buoyancy effect relatively weak. This is due to the weaker buoyancy effects for the system with a smaller $(1+N)$.

The distributions of temperature and concentration

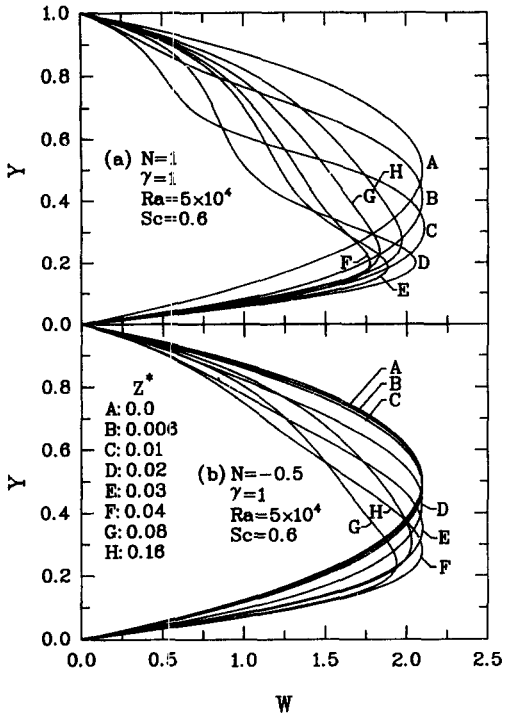

Fig. 11. The distributions of axial velocity profiles.

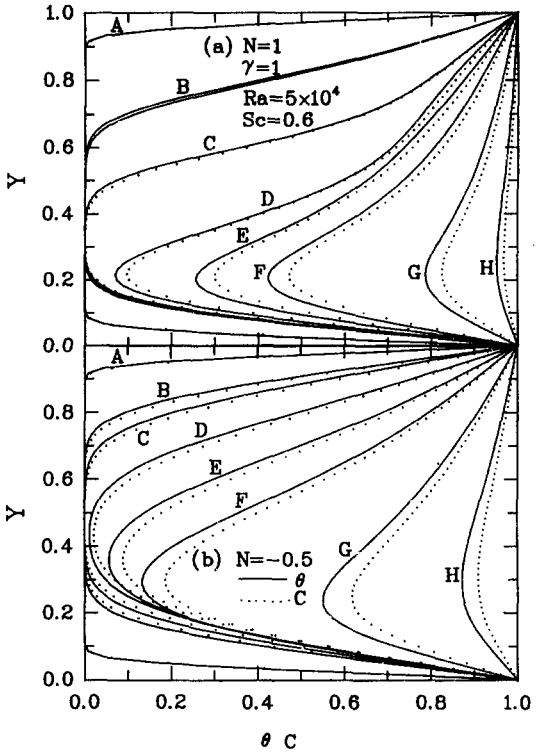

Fig. 12. The developments of temperature and concentration profiles.

profiles are of interest in understanding the characteristics of heat and mass transfer. The typical developing temperature and concentration profiles along vertical center plane $x = a/2$ are presented in Fig. 12. The buoyancy-driven secondary flow carries the heated fluid upward along the side walls and downward along the center region of the duct. Therefore, temperature and concentration gradients at the lower wall ($Y = 0$) are greater than those at the upper wall ($Y = 1$). The locations of minimum θ or C are shifted toward the upper wall as the buoyancy ratio N is decreased. This is clearly shown in Fig. 12(b). An overall inspection of Fig. 12 reveals that both θ and C develop in a very similar fashion. Additionally, the concentration boundary layers develop a little more rapidly than the temperature boundary layers do. This is attributed to the fact that Sc ($= 0.6$) is smaller than Pr ($= 0.7$) in the flow.

5. CONCLUSION

Laminar mixed convection flows in horizontal rectangular ducts under the simultaneous influences of combined buoyancy effects of thermal and mass diffusion have been studied. The effects of the Rayleigh number Ra, buoyancy ratio N, Schmidt number Sc and aspect ratio γ on the momentum, heat and mass transfer were examined in detail. What follows is brief summary of the major results.

(1) Under the ranges of the governing parameters investigated in this work, the free convection effect is practically negligible only when $Ra \leqslant 5 \times 10^2$.

(2) The distributions of local Nusselt (Sherwood) number are characterized by a decay near the entrance due to the entrance effect; but the decay is attenuated by the onset of buoyancy-driven secondary flows. After a first local minimum being reached, the values of Nu (Sh) increase to a local maximum at an axial location where the buoyancy effects are the most intense. Finally, the Nu (Sh) falls asymptotically to the Graetz solution value as the fully developed situation is attained.

(3) The local friction factor, Nusselt number and Sherwood number are enhanced as the buoyancy force from species diffusion assists the thermal buoyancy force.

(4) Better heat and mass transfer is noted for a channel with a smaller aspect ratio.

(5) The buoyancy-driven secondary flow distorts the axial velocity, temperature and concentration distributions and the nature of the distribution depends on the magnitude of Ra and N.

Acknowledgements—The author would like to acknowledge the financial support of the present work by the National Science Council, R.O.C., through contract NSC 82-0401-E211-003.

REFERENCES

1. K. C. Cheng and G. J. Hwang, Numerical solution for combined free and forced laminar convection in horizontal rectangular channels, *J. Heat Transfer* **91**, 59–66 (1969).
2. F. C. Chou and G. J. Hwang, Combined free and forced

laminar convection in horizontal rectangular channels for high *ReRa*, *Can. J. Chem. Engng* **62,** 830–836 (1984).
3. S. Ostrach and Y. Kamotani, Heat transfer augmentation in laminar fully developed channel flow by means of heating from below, *J. Heat Transfer* **97,** 220–225 (1975).
4. K. C. Cheng, S. W. Hong and G. J. Hwang, Buoyancy effects on laminar heat transfer in the thermal entrance region of horizontal rectangular channels with uniform wall heat flux for large Prandtl number fluid, *Int. J. Heat Mass Transfer* **15,** 1819–1836 (1972).
5. J. W. Ou, K. C. Cheng and R. C. Lin, Natural convection effects on Graetz problem in horizontal rectangular channels with uniform wall temperature for large *Pr*, *Int. J. Heat Mass Transfer* **17,** 835–843 (1974).
6. K. C. Cheng and J. W. Ou, Convection instability and finite amplitude convection in the entrance region of horizontal rectangular channels heated from below, *Proceedings of 7th International Heat Transfer Conference* Vol. 2, pp. 189–194 (1982).
7. C. A. Hieber and S. K. Sreenivasan, Mixed convection in an isothermally heated horizontal pipe, *Int. J. Heat Mass Transfer* **17,** 1337–1348 (1974).
8. S. W. Hong, S. M. Morcos and A. E. Bergles, Analysis and experimental results for combined forced and free laminar convection in horizontal tubes, *Proceedings of the 5th International Heat Transfer Conference*, Vol. 3, pp. 154–158 (1974).
9. J. W. Ou and K. C. Cheng, Natural convection effects on Graetz problem in horizontal isothermal tubes, *Int. J. Heat Mass Transfer* **20,** 953–960 (1977).
10. M. Hishida, Y. Nagano and M. S. Montesclaros, Combined forced and free convection in the entrance region of an isothermally heated horizontal pipe, *J. Heat Transfer* **104,** 153–159 (1982).
11. M. M. M. Abou-Ellail and S. M. Morcos, Buoyancy effects in the entrance region of horizontal rectangular channels, *J. Heat Transfer* **105,** 924–928 (1983).
12. F. P. Incropera and J. A. Schutt, Numerical simulation of laminar mixed convection in the entrance region of horizontal rectangular ducts, *Numer. Heat Transfer* **8,** 707–729 (1985).
13. H. V. Mahaney, F. P. Incropera and S. Ramadhyani, Development of laminar mixed convection flow in a horizontal rectangular duct with uniform bottom heating, *Numer. Heat Transfer* **12,** 137–155 (1987).
14. F. C. Chou and G. J. Hwang, Vorticity-velocity method for Graetz problem with the effect of natural convection in a horizontal rectangular channel with uniform wall heat flux, *J. Heat Transfer* **109,** 704–710 (1987).
15. F. C. Chou and G. J. Hwang, Numerical analysis of the Graetz problem with natural convection in a uniformly heated horizontal tube, *Int. J. Heat Mass Transfer* **31,** 1299–1308 (1988).
16. J. N. Lin and F. C. Chou, Laminar mixed convection in the thermal entrance region of horizontal isothermal rectangular channels, *Can. J. Chem. Engng* **67,** 361–367 (1989).
17. J. N. Lin, F. C. Chou and P. Y. Tzeng, Theoretical prediction of the onset of thermal instability in the thermal entrance region of horizontal rectangular channels, *Int. J. Heat Fluid Flow* **12,** 218–224 (1991).
18. G. J. Hwang and C. L. Liu, An experimental study of convective instability in the thermal entrance region of a horizontal parallel plate channel heated from below, *Can. J. Chem. Engng* **54,** 521–525 (1976).
19. Y. Kamotani, O. Ostrach and H. Miao, Convective heat transfer augmentation in thermal entrance regions by means of thermal instability, *J. Heat Transfer* **101,** 222–226 (1979).
20. J. R. Maughan and F. P. Incropera, Experiments on mixed convection heat transfer for airflow in a horizontal and inclined channel, *Int. J. Heat Mass Transfer* **30,** 1307–1318 (1987).
21. F. Santarelli and F. P. Foraboschi, Heat transfer in laminar mixed convection in a reacting fluid, *Chem. Engng* **6,** 59–68 (1973).
22. T. F. Lin, C. J. Chang and W. M. Yan, Analysis of combined buoyancy effects of thermal and mass diffusion on laminar forced convection heat transfer in a vertical tube, *J. Heat Transfer* **110,** 337–344 (1988).
23. J. N. Lin, F. C. Chou, W. M. Yan and P. Y. Tzeng, Combined buoyancy effects of thermal and mass diffusion on laminar forced convection in the thermal entrance region of horizontal square channels, *Can. J. Chem. Engng* **79,** 681–689 (1992).
24. B. Gebhart and L. Pera, The nature of vertical natural convection flows resulting from the combined buoyancy effects of thermal and mass diffusion, *Int. J. Heat Mass Transfer* **14,** 2025–2050 (1971).
25. T. S. Chen and C. F. Yuh, Combined heat and mass transfer in natural convection along a vertical cylinder, *Int. J. Heat Mass Transfer* **23,** 451–461 (1980).
26. K. Ramakrishna, S. G. Rubin and P. K. Khosla, Laminar natural convection along vertical square ducts, *Numer. Heat Transfer* **5,** 59–79 (1982).
27. P. J. Roache, *Computational Fluid Dynamics*, pp. 61–64. Reinhold, New York (1971).
28. R. A. Shah and A. L. London, Laminar flow forced convection in ducts, Suppl. 1 to *Adv. Heat Transfer* [Suppl. 1], pp. 196–222. Academic Press, New York (1978).